

Theoretical Study of Solid/Solid Interfaces in All-solid-state Batteries

Abstract

All-solid-state batteries (ASSBs) are widely investigated as promising energy storage systems with potentially high safety and design flexibility. Main problems to be overcome to bring current ASSBs into real applications are their poor cyclability as well as low energy density. These problems can be solved by using high-energy-density cathodes with higher stabilities. Ni-rich cathodes such as bare and doped $\text{LiNi}_x\text{Mn}_y\text{Co}_z\text{O}_2$ (NMC) and $\text{LiNi}_x\text{Co}_y\text{Al}_z\text{O}_2$ (NCA) are promising candidates for these purposes. In this project, we aim to find effect of doping on the chemical and mechanical stability of these cathode materials as well as their interfaces with solid electrolytes such as $\text{Li}_7\text{La}_3\text{Zr}_2\text{O}_{12}$ (LLZO) using *ab initio*-based approaches. Last year, we studied effect of B doping on surface structure and stability of a Ni-rich NCA cathode and its microstructure, mechanical stability of a bare Ni-rich NMC cathode, cation interchange between the Ni-rich NMC and LLZO, and grain boundaries (GBs) of the bare LNO. In this year's project, we aim to continue our study by finding the effect of Ti, F, and N dopants on defect formation (chemical stability) and mechanical stability of NMC811 cathodes. In particular, we will model, for the first time, GB interfaces in NMC811 microstructures and study effect of the aforementioned dopants on properties of GBs.

1. Organizational details

Title of the project:

Theoretical Study of Solid/Solid Interfaces in All-solid-state Batteries

Project leaders:

Dr. Payam Kaghazchi

Institut für Energie und Klimaforschung IEK-1: Werkstoffsynthese und
Herstellungsverfahren

Forschungszentrum Jülich GmbH

D-52425 Jülich

payam.kaghazchi@fu-berlin.de

Project administrator:

Najma Yaqoob

Institut für Energie und Klimaforschung IEK-1: Werkstoffsynthese und
Herstellungsverfahren

Forschungszentrum Jülich GmbH

D-52425 Jülich

n.yaqoob@fz-juelich.de

2. Introduction

All solid-state batteries (ASSBs) hold the promise of overcoming the current constraints of conventional battery technologies such as limited long-term-stability and safety. They are currently regarded as the next, revolutionary step in electrochemical energy storage. However, achieving the targets of high-stability and high-energy density solid-state batteries poses significant challenges and requires rational design of all components to increase capacity and minimize resistances. LiMO_2 ($M = \text{Ni, Co, Mn, and/or Al}$) compositions are among the most promising cathode materials for Li-based batteries [1,2]. In particular, Ni-rich LiMO_2 cathodes deliver not only a large capacity [3-6] but also decrease the battery cost by reducing the use of expensive Co. However, the high capacity of Ni-rich LiMO_2 is accompanied by poor cycling performance arising from microcracks that form inside the cathode microstructures upon the deeply charged states [7]. To improve the cycling stability, it is necessary to reduce the formation of cracks, which is induced by the large lattice size variation during charge/discharge [8]. Doping and substitution are promising strategies to improve the performance of cathodes [9-14]. Modeling and simulation using density functional theory (DFT) calculation have been applied to study the occupation site, mechanism of charge compensation, and solubility of some types of dopants as well as effect of some dopants on electronic and ionic conductivity, and volume change of battery materials (for example please see refs. [15-21]). In our previous projects supported by HLRN, we have studied the effect of Zr- [22], W- [23], and B-doping [24] on LiNiO_2 (LNO) as well as Fe in NaMnO_2 cathode materials [25]. For example, we determined the mechanism of charge compensation and lattice parameter change for Zr-doped LNO [22] and surface structure and stability for W-doped LNO [23]. However, effect of doping on surface and mechanical stability of Ni-rich LiMO_2 microstructures had not been investigated. Last year, we simulated, for the first time, effect of B doping on the stability of a Ni-rich LiMO_2 cathode material ($\text{Li}[\text{Ni}_x\text{Co}_y\text{Al}_{1-x-y}]\text{O}_2$, so called NCA89) [26], which will be discussed in the next section. Our simulations, in agreement with experimental results, indicate that B dopants prefer to occupy the surface of NCA89. It was found that B dopants by tailoring the morphology of microstructures can improve the cyclability of NCA89. However, the effect of some other types of dopants, which typically occupy bulk sites, on defect formation and mechanical stability is unknown. On the other hand, $\text{Li}_7\text{La}_3\text{Zr}_2\text{O}_{12}$ (LLZO) is the most widely-studied oxide-based solid electrolyte for ASSBs [23]. Electronic and atomic structure as well as Li ion transport in LLZO bulk with and without doping have been also studied extensively by applying DFT and *ab initio* molecular dynamics (AIMD) calculations [27-29]. Elastic constants of bare LLZO has been calculated using DFT calculations [30]. However, effect of doping, in particular with Al and Ta which are necessary to stabilize and improve Li ionic conductivity of LLZO, on elastic constants which determine mechanical stability of LLZO have not been addressed so far. Defect chemistry in LLZO has also been studied using experimental [31, 32] and theoretical [33] methods. In particular, we have recently studied Li and O vacancy formation energy in Al-doped LLZO that is, in practice, used in ASSBs [34]. Besides bulk properties, surface and nanoparticle structures [35] as well as grain boundaries (GBs) [36] of bare LLZO have been modelled and studied using DFT and AIMD. However, defect formation and mechanical stability in practical solid-state electrolytes, namely Al-LLZO and Ta-LLZO, have not been studied so far. Recently, for the first time, we simulated the atomic structure of interfaces between LLZO and a cathode material [37]. In that study we focused on the LiCoO_2 (LCO) cathode. The atomic and electronic structure of interface between Ni-rich LiMO_2 and LLZO have not been simulated. In addition, the strength of interfaces in ASSBs has not been simulated so far. In this project, by applying DFT calculations, we aim to model and study effect of (i) Ti, F, and N doping on defect formation and mechanical stability of bulk (WP1) and GBs (WP2) of an interesting cathode material, namely $\text{Li}[\text{Ni}_{0.8}\text{Co}_{0.1}\text{Mn}_{0.1}]\text{O}_2$ (NCM811). The next logical steps after this project will be to study effect of doping on mechanical properties of LLZO bulk and GBs as well as chemical and mechanical stability of NCM811/LLZO interfaces for ASSBs. In the following, we summarize our obtained results from **01.07.2019** to **27.04.2020** and then in the next section we discuss our strategy to continue this project.

WP. 1 Calculate surface free energies of pristine and Me-doped NMC using DFT calculations

To investigate the effect of doping on stability of Ni-rich LiMO₂ cathodes, we simulated both surface and mechanical stabilities. Motivated by measurements of our experimentalist partner on Ni-rich Li[Ni_xCo_yAl_{1-x-y}]O₂ cathodes, we calculated surface free energies of pristine LiNi_{0.92}Co_{0.04}Al_{0.04}O₂ (P-NCA89) and B-doped LiB_{0.02}Ni_{0.90}Co_{0.04}Al_{0.04}O₂ (B-NCA88). To investigate the surface energy modification by B doping, we compared stabilities of P-NCA89 and B-NCA88 surfaces by calculating the surface energies of (003), (01-2), (104), and (100) surfaces using DFT. Surface energies were computed by:

$$\gamma = \frac{1}{2A} [E_{\text{surf}} - E_{\text{bulk}} + (N_{\text{Ni}} - N_{\text{Li}})\mu_{\text{Li}}]. \quad (1)$$

Here, E_{surf} and E_{bulk} are the total energy of surface and bulk structure, respectively. N_{Ni} and N_{Li} are number of Ni and Li in the surface. μ_{Li} is the chemical potential of Li, and A is the surface area of the slab. For all surfaces, we modelled non-polar stoichiometric structures. A reconstructed structure was considered for the stoichiometric (003) surface to stabilize it. Moreover, we modelled non-polar nonstoichiometric (003) and (012) surfaces with deficiency and excess of Li at the topmost layers. The B dopant was considered to occupy the subsurface layers. Figure 1 shows γ as function of $\Delta\mu_{\text{Li}}$ (referenced to the total energy per atom of a metal Li reservoir) for bare LiNi_{0.92}Co_{0.04}Al_{0.04}O₂ and B-doped LiB_{0.02}Ni_{0.90}Co_{0.04}Al_{0.04}O₂ surfaces. The low and high values of $\Delta\mu_{\text{Li}}$ represent Li-poor and -rich conditions, respectively. For $\Delta\mu_{\text{Li}} \leq -3.67$ eV, the Li-poor bare LiNi_{0.92}Co_{0.04}Al_{0.04}O₂ (003) surface becomes the most stable since it has the lowest value of γ . The stoichiometric B-doped LiB_{0.02}Ni_{0.90}Co_{0.04}Al_{0.04}O₂ (104) surface becomes the most favorable one for -3.67 eV $\leq \Delta\mu_{\text{Li}} \leq -2.85$ eV. However, for -2.85 eV $\leq \Delta\mu_{\text{Li}}$, the non-stoichiometric Li-rich B-doped LiB_{0.02}Ni_{0.90}Co_{0.04}Al_{0.04}O₂ (003) surface with a well-ordered layer of lithium boron oxide structure is the most stable surface. Three O anions from the subsurface layer with the B dopant forms a Li₃BO₃ layer. The calculated average B-O bond length, which is 1.387 Å, is close to the value of 1.377 Å in the α -Li₃BO₃ phase measured by a previous experimental study. Furthermore, it was found that B-doped (012) can form. Our calculations confirm the presence of (003), (104), and (012) facets on the primary particles of B-doped LiB_{0.02}Ni_{0.90}Co_{0.04}Al_{0.04}O₂ microstructures. In addition, to study the effect of tailoring of microstructure on its stability during Li extraction, the stress distribution was calculated using

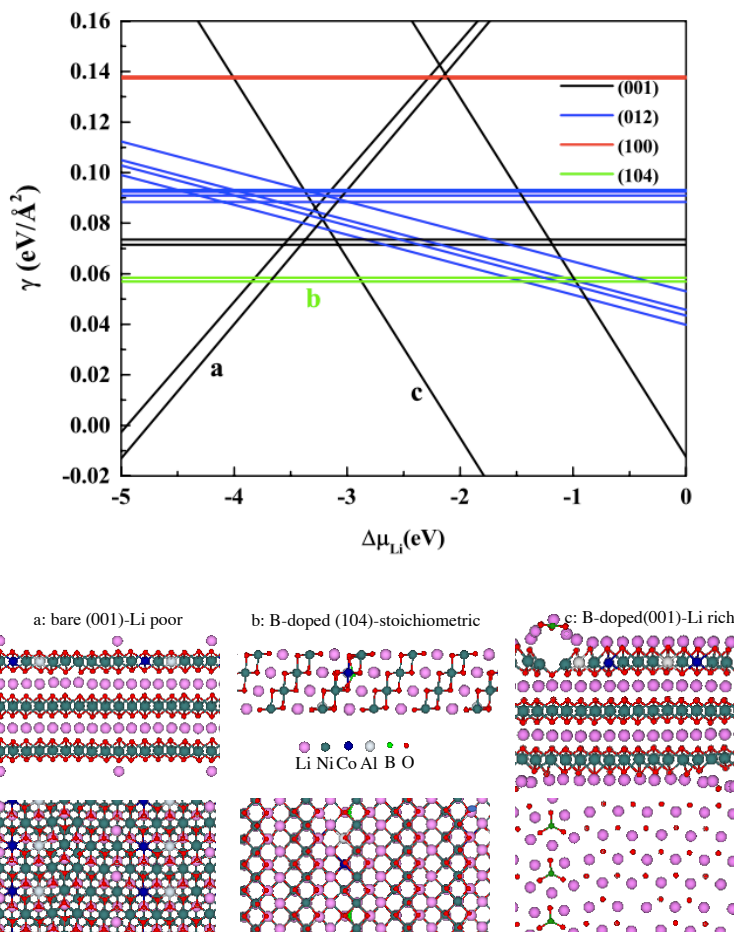


Fig. 1 (top) Surface energies of bare and B-doped LiNi_{0.9}Co_{0.04}Al_{0.04}O₂(001), (012), (100), and (104) surfaces as function of the chemical potential of Li ($\Delta\mu_{\text{Li}}$) referenced to bulk metal Li. (bottom) Most favorable surface structures at different values of $\Delta\mu_{\text{Li}}$.

a finite element simulation. We found that the stresses are significantly smaller for the doped B-NCA88 material in all cases. The shell part of the B-NCA88 particle is rather stress-free, which enhances its integrity during cycling. The results of our study have been published in the journal of Materials Today [26].

After discussion with our experimentalist partners, we realized that elastic constants and strength as function of Li concentration in bulk and GBs of cathode and electrolyte materials are important parameters to control the stability of cathodes. Thus, we continued this work by calculating these quantities for LCO and LNO bulk, i.e. reference cathode systems, as well as Ni-rich NCM811 bulk. Our calculated elastic constants and strength for LCO, for example, agree well with the experimental data. Figure 2 shows computed uniaxial stress along the *c* direction as function of strain for $\text{Li}_{0.5}\text{CoO}_2$. Our calculation clearly shows that during charge or discharge a lattice-parameter-variation-induced stress of 4.5 GPa can lead to the formation of cracks in LCO cathodes. We are now computing these quantities for NCM811 bulk. A comparison between our results for bare NCM811 bulk with those for doped ones (continuation of this project) will show how doping can affect crack formation in Ni-rich cathode materials. We are preparing a manuscript on this project.

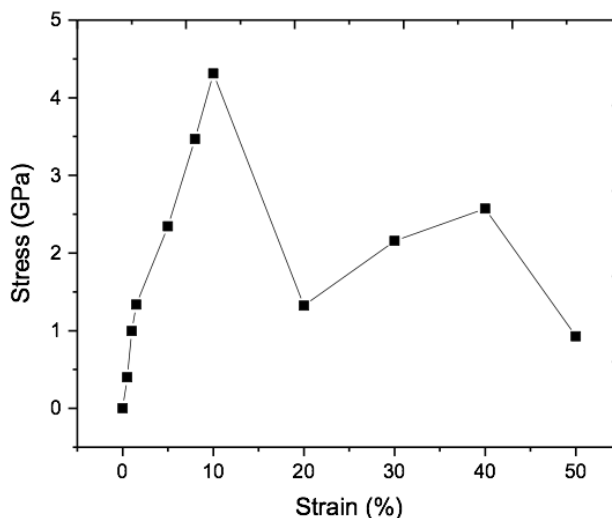


Fig. 2 Calculated tensile uniaxial stress along the *c* direction as function of strain in $\text{Li}_{0.5}\text{CoO}_2$ bulk.

WP2. Modeling of space charge at LLZO/NMC

Before modeling the space charge, we have to determine the structure of cathode/electrolyte interface. The first step in this direction is to study the initial stage of interaction between cathode and electrolyte, namely cation interchange between them. Motivated by our experimentalist partners in IEK-1, we first focused on the cation interchange process between LCO and LLZO as well as NCM811 and LLZO. Instead of working on the proposed types of dopants, we considered the LCO and bare NCM811 systems because our experimentalist partners have focused on these cathodes materials. Another reason was that, as mentioned in the previous WP, we found that B dopants occupy surface sites and not bulk, and therefore cation interchange cannot be affected by B doping.

The interchange energies E_i for a variety of possible cation interchanges between LCO and LLZO as well as NCM811 and LLZO were computed as listed in Tab. 1. Interestingly, we find that the interchange energy between any TM cation in the cathode and Al dopant in the Li site of LLZO is negative, meaning a spontaneous reaction between cathode and Al-doped LLZO. This means that during high-temperature processing of LCO/Al-LLZO or NCM811/Al-LLZO mixed cathodes we can have TM cation migration from cathode into LLZO. Further experimental measurements are in progress to find the complex structure of the interface in our ASSBs. We are now calculating E_i as function of Li concentration

Tab. 1 Calculated cation interchange energies in eV between LCO and Al-LLZO as well as NCM811 and Al-LLZO

LCO	Interchange energy (eV)		
	Co ↔ La	Co ↔ Zr	Co ↔ Al
	5.11	2.97	-0.44
NCM811	Ni ↔ La	Ni ↔ Zr	Ni ↔ Al
	5.21	3.47	-1.19
	Co ↔ La	Co ↔ Zr	Co ↔ Al
	5.42	3.25	-1.23
	Mn ↔ La	Mn ↔ Zr	Mn ↔ Al
	7.77	2.90	-1.10

in cathodes to investigate the stability of cathode/electrolyte interfaces as function of level of charge/discharge. The results of this study together with experimental measurements will be an important step toward understanding the NCM811/Al-LLZO interface structure and will be published in a prestigious journal.

Recently, our experimentalist partners have found that it is not only the cathode/electrolyte interface but also the GBs in the cathode and electrolyte microstructures play important roles in determining the stability of ASSBs. For this reason, we started to investigate GBs. We first focused on LNO as a model system for Ni-rich cathode materials. Figure 3 shows a simulated tilt $\Sigma 3[11-20](1-102)$ GB of LNO. We performed an extensive number of simulations to find the minimum energy structure of this GB as function of Li concentration. We are now calculating the formation energy, electronic structure, and strength of this GB. The aim is to find the impact of GB on chemical and mechanical stability of microstructures of cathodes. A comparison between our results on bare GBs with those on doped ones (continuation of this project) will show how doping can affect the performance of cathode microstructures.

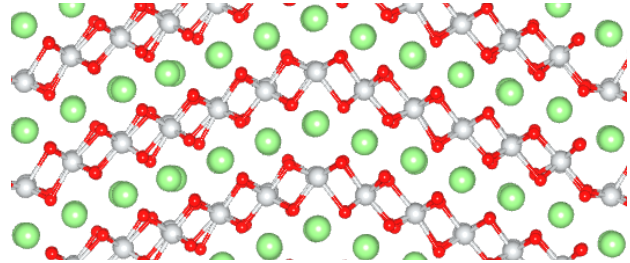


Fig. 3 Side view of atomic structure of tilt $\Sigma 3[11-20](1-102)$ GB of bare LNO with full Li concentration.

3. Project description and computational details

Last year, we simulated surface energies and mechanical stabilities of B-doped Ni-rich NCA cathode materials. In the continuation of this project, we aim to study effect of doping on defect formation energies and mechanical properties of $\text{LiNi}_{0.8}\text{Mn}_{0.1}\text{Co}_{0.1}\text{O}_2$ (NMC811) cathodes for Li-based battery applications. Our last year experiences and discussions with experimental collaborators show that some of the most interesting doping elements are Ti, F, and N. The first one occupies a TM site, while the last two occupy O sites. We will focus on $\text{Li} \leftrightarrow \text{Ni}$ antisite and O vacancy defects. Their formation energies will be calculated using the following equations, respectively:

$$E_{\text{F}}^{\text{antisite}} = E_{\text{tot}}^{\text{Li} \leftrightarrow \text{Ni}} - E_{\text{tot}}^{\text{pristine}}, \quad (2)$$

and

$$E_{\text{F}}^{\text{V}_\text{O}} = E_{\text{tot}}^{\text{V}_\text{O}} - E_{\text{tot}}^{\text{pristine}} - \frac{1}{2} E_{\text{tot}}^{\text{O}_2}, \quad (3)$$

where $E_{\text{tot}}^{\text{Li} \leftrightarrow \text{Ni}}$, $E_{\text{tot}}^{\text{pristine}}$, $E_{\text{tot}}^{\text{V}_\text{O}}$ are the total energies of NCM811 bulk (or GB) with a $\text{Li} \leftrightarrow \text{Ni}$ interchange defect, without any defect, and with a single O vacancy, respectively. $E_{\text{tot}}^{\text{O}_2}$ is the total energy of a single O_2 molecule. We will use Perdew-Burke-Ernzerhof (PBE) [38] and SCAN [39] functional. Our recent studies show that SCAN can predict electronic structure even better than PBE+ U for different Li concentrations without having the tunable U parameter. To calculate $E_{\text{F}}^{\text{antisite}}$ and $E_{\text{F}}^{\text{V}_\text{O}}$ for bare and doped NMC811 bulk, we will consider a $4 \times 4 \times 1$ supercell. We will focus on Li concentrations of 1.00, 0.75, 0.50, 0.25, and 0.00. We will study concentrations of ~ 3 , 6, and 12 percent of Ti, F, and N dopants. We will fully optimize unit cell parameters and geometries using $2 \times 2 \times 1$ k-points and energy cutoff of 500 eV. To calculate total energies and stresses which are needed to compute elastic constants and strengths, we will use the same set up as before but we will keep the unitcells fixed.

We need a set of calculated total energies and stresses for geometry optimized structures with various unit cells. We will then use a finite difference method implemented in a home-developed Python code with the obtained DFT data to calculate elastic constants. To compute $E_F^{\text{antite}} and E_F^{Vo} for bare and doped tilt $\Sigma 3[11-20](1-102)$ GB of NMC811, we will consider a $2 \times 1 \times 1$ supercell. We will focus on Li concentrations of 1.00, 0.75, 0.50, 0.25, and 0.00. We will only study the concentration of ~ 3 percent of Ti, F, and N dopants. We will fully optimize unit cell parameters and geometries using $4 \times 4 \times 1$ k-points and energy cutoff of 500 eV. To compute total energies and stresses for elastic constants and strength calculations, we will use the same set up as before but we will keep the unitcells fixed.$

4. Work plan

WP1. Determine effect of doping on defect formation and mechanical properties of NCM811 bulk

We will calculate formation energies of Li \leftrightarrow Ni interchange and O vacancy defects for Ti-doped, F-doped, and N-doped Li $_x$ NMC811 as function of Li concentration. Similar to the already-simulated bare case, we will focus on 5 various Li concentrations, namely $x=1.00, 0.75, 0.50, 0.25,$ and 0.00 . We will first perform Coulomb energy calculations for each dopant type and concentration and each Li concentration. Since there is only one possible configuration for the cases of $x=1.00$ and 0.00 , Coulomb energy calculations will only be performed for $x=0.75, 0.50,$ and 0.25 . After carrying out Coulomb energy calculations, we will list the energies and will perform DFT-PBE calculation on 20 lowest-energy structures. After determining the minimum total energy structures, we will calculate defect formation energies as function of dopant type and concentration as well as Li concentration. Finally, we will compute elastic constants using our Python code as well as tensile and compressive strengths for Ti-doped, F-doped, and N-doped Li $_x$ NMC811 systems. The aim of this project is to determine effect of cation and anionic doping on defect formation and strength of cathode materials in ASSBs. Finally, we will recalculate the electronic structures with the SCAN functional. These calculations will show how oxidation states and magnetization will be affected by the type of the exchange-correlation functional.

WP2. Find effect of doping on defect formation and mechanical properties of grain boundary interfaces of NCM811 microstructures

In this work package, we will model GB interfaces in bare and doped NCM811 microstructures. To achieve this aim, we will focus on the tilt $\Sigma 3[11-20](1-102)$ GB that we modelled in the previous project for LNO. To find the most stable structure of the GB as function of Li in bare Li $_x$ NMC811, we will first consider Li $_x$ NMC811 with $x=1.00$ and perform 20 DFT-PBE calculations on various possible arrangements of Ni, Mn, and Co. We will also use our gained knowledge on the structure of Li $_x$ NMC811 bulk. After determining the atomic structure of $\Sigma 3[11-20](1-102)$ GB of Li $_{1.00}$ NMC811, we will find the arrangement of Li ions in $\Sigma 3[11-20](1-102)$ GB of Li $_x$ NMC811 with $x=0.75, 0.50$ and 0.25 . Please note that there is only one configuration for $x=0.00$. Afterwards, we will calculate atomic and electronic structures of the GB as function of type of dopant and Li concentration. After determining the minimum energy structures, we will compute defect formation energies and strengths of the GBs as function of dopant and Li concentrations. In this case, to save the computing time and also to study the possibility of segregation of dopant into the GB interface, we will focus on the lowest concentration case. We will finally recalculate the electronic structures of the most favourable structures using the SCAN functional.

5. Resource request

In our proposal for 2016-2017, we carried out geometry-optimization calculations for LCO cathode using different number of cores and processors and plotted speedup curves. Based on this curve and our recent calculations, I will give the details of the required number of core-hours for performing our project.

WP1. We will simulate **3** different concentrations of **3** types of dopants and **20** configurations of **3** Li concentrations ($x=0.75, 0.50, \text{ and } 0.25$). There is only **1** possible configuration for each of the **2** following cases of $x=1.00$ and 0.00 . Based on our experience on pristine NCM811 system, each full optimization DFT-PBE calculation (with the computational set up as mentioned above) using **96** cores needs **18** hours in average. This means that we need $3*3*20*3*96*18+3*3*2*1*96*18=964224$ core hours. We will then compute formation energies of **2** defective cases, namely antisite and O vacancy, by studying **5** possible configurations for **3** different concentrations of **3** types of dopants and **5** Li concentrations. Since the same computing time as the previous step is expected, we need the following computing time: $2*5*3*3*5*96*18=777600$ core hours. Afterwards, we will compute elastic constants. Based on our experience for the bare NCM811 bulk, the elastic constants can be computed with 25 single point (without geometry and unit cell optimization) calculations which with **96** cores it takes in average about **12** hours. This means that for **3** different concentrations of **3** types of dopants for **5** different Li concentrations we need $3*3*5*96*12=51840$ core hours. Moreover, we will calculate tensile and compressive (**2** sets of calculations) strengths of $\text{Li}_x\text{NMC811}$ along **2** directions with **3** different concentrations of **3** types of dopants for **5** Li concentrations by performing geometry optimization for **10** different lattice parameters. Since each geometry relaxation calculation for NCM811 bulk requires **96** cores and **3** hours we need $2*2*3*3*5*10*96*3=518400$ core hours. We will finally recalculate the electronic structures with SCAN by focusing on the determined structures with PBE. Since we start with PBE results the computing time is not very long and it is similar to the PBE one: $3*3*5*96*18=77760$ core hours. We will, therefore, need the following resources for this WP: $964224+777600+51840+518400+77760=2389824$ core hours (about **199152** NPL).

WP2. To find the arrangement of TMs in the GB of $\text{Li}_{1.00}\text{NMC811}$, we will perform **20** DFT-PBE calculations. Based on our calculation for the GB of LNO with **96** cores, one simulation will take **18** hours. We will therefore need $20*96*18=34560$ core hours. To simulate **1** concentration (the lowest one) of **3** types of dopants in the GB of $\text{Li}_x\text{NMC811}$ with **3** Li concentrations ($x=0.75, 0.50, \text{ and } 0.25$) we have to find the most favorable configuration of Li arrangement for each case by performing **20** DFT-PBE calculations. There is only **1** possible configuration for the case of $x=0.00$. We need the same computing time as the previous step for each case. This means that we need $1*3*3*20*96*18+1*3*1*1*96*18=316224$ core hours. We will then compute antisite and O vacancy formation energies for **1** concentration (the lowest one) of **3** types of dopants as well as the bare case ($1*3+1=4$) with **5** Li concentrations. Since we have to find the most favorable configuration of O vacancy and $\text{Ni}\leftrightarrow\text{Li}$ arrangement for each case by performing **10** DFT-PBE calculations we will need: $4*5*10*96*18=345600$ core hours. Afterwards, we will calculate tensile and compressive (**2** sets of calculations) strengths along the GB normal direction for pristine and doped $\text{Li}_x\text{NMC811}$ GBs cases (**4** systems) with **5** Li concentrations by performing geometry optimization for **10** different lattice parameters. Since each geometry optimization takes in average **5** hours (based on our calculations for the GB of LNO) we will need $2*4*5*10*96*5=192000$ core hours. We will finally perform DFT-SCAN calculation for $1*3+1=4$ systems with **5** Li concentrations: $4*5*96*18=34560$. Therefore, we need $34560+316224+345600+192000+34560=922944$ core-hours (about **76912** NPL).

Milestones	required core hours	required NPL
WP1. Determine effect of doping on defect formation and mechanical properties of NCM811 bulk	2389824	199152
WP2. Find effect of doping on defect formation and mechanical properties of grain boundary interfaces of NCM811 microstructures	922944	76912
Total required core hours or NPL for 1 year	3312768	276064

References

- [1] J. R. Dahn, U. V. Sacken and C. A. Michal, *Solid State Ionics*, 1990, 44, 87-97.
- [2] L. Biasi, A. O. Kondrakov, H. Geßwein, T. Brezesinski, P. Hartmann and J. Janek, *J. Phys. Chem. C*, 2017, 121, 26163-26171.
- [3] H.-J. Noh, S. Youn, C. S. Yoon and Y. K. Sun, *J. Power Sources*, 2013, 233, 121-130.
- [4] J.-H. Kim, H.-H. Ryu, S. J. Kim, C. S. Yoon and Y.-K. Sun, *ACS Appl. Mater. Interfaces*, 2019, 11, 30936-30942.
- [5] H.-H. Ryu, K.-J. Park, C. S. Yoon and Y.-K. Sun, *Chem. Mater.*, 2018, 30, 1155-1163.
- [6] C. S. Yoon, D.-W. Jun, S.-T. Myung and Y.-K. Sun, *ACS Energy Lett.*, 2017, 2, 1150-1155.
- [7] H.-H. Ryu et al., *Chem. Mater.* 30 (2018) 1155–1163.
- [8] U.-H. Kim, H.-H. Ryu, J.-H. Kim, R. Mücke, P. Kaghazchi, C. S. Yoon and Y.-K. Sun, *Adv. Energy Mater.*, 2019, 9, 803902.
- [9] H. Buschmann, J. Dölle, S. Berendts, A. Kuhn, P. Bottke, M. Wilkening, P. Heitjans, A. Senyshyn, H. Ehrenberg, A. Lotnyk, V. Duppel, L. Kienlee and J. Janek, *Phys. Chem. Chem. Phys.*, 2011, 13, 19378-19392.
- [10] H. E. Shinawi and J. Janek, *J. Power Sources*, 2013, 225, 13-19.
- [11] M. Matsui, K. Takahashi, K. Sakamoto, A. Hirano, Y. Takeda, O. Yamamoto and N. Imanishi, *Dalton Trans.*, 2014, 43, 1019-1024.
- [12] H. Tukamoto and A. R. West, *J. Electrochem. Soc.*, 1997, 144, 3164-3168.
- [13] A. Rougier, I. Saadoun, P. Gravereau, P. Willmann and C. Delmas, *Solid State Ionics*, 1996, 90, 83-90.
- [14] C. S. Yoon, M.-J. Choi, D.-W. Jun, Q. Zhang, P. Kaghazchi, K.-H. Kim and Y.-K. Sun, *Chem. Mater.*, 2018, 30, 1808-1814.
- [15] Y. Koyama, H. Arai, I. Tanaka, Y. Uchimotoc and Z. Ogumi, *J. Mater. Chem. A*, 2014, 2, 11235-11245.
- [16] S. Kim, S. Choi, K. Lee, G. J. Yang, S. S. Lee and Y. Kim, *Phys. Chem. Chem. Phys.*, 2017, 19, 4104-4113.
- [17] K. Hoang, *Phys. Rev. Mater.*, 2017, 1, 075403-075412.
- [18] S. Shi, C. Ouyang, M. Lei and W. Tang, *Journal of Power Sources*, 2007, 171, 908-912.
- [19] F. Ning, B. Xu, J. Shi, M. Wu, Y. Hu and C. Ouyang, *J. Phys. Chem. C*, 2016, 120, 18428-18434.
- [20] S. Hao, N. Zhao, C. Shi, C. He, J. Li and E. Liu, *Ceramics International*, 2015, 41, 2294-2300.
- [21] H. Chen, J. A. Dawson and J. H. Harding, *J. Mater. Chem. A*, 2014, 2, 7988-7996.
- [22] C. S. Yoon, Q. Zhang, P. Kaghazchi and Y.-K. Sun, *Chem. Mater.* 2018, 30, 1808-1814.
- [23] U.-H. Kim, D.-W. Jun, K.-J. Park, Q. Zhang, P. Kaghazchi, D. Aurbach, D. T. Major, G. Goobes, M. Dixit, N. Leifer, C. M. Wang, P. Yan, D. Ahn, K. H. Kim, C. S. Yoon and Y.-K. Sun, *Energy Environ. Sci.*, 2018, 11, 1271-1279.
- [24] K.-J. Park, H.-G. Jung, L.-Y. Kuo, P. Kaghazchi, C. S. Yoon and Y.-K. Sun, *Advanced Energy Materials*, 2018, 8, 1801202.
- [25] J. U. Choi, Y. J. Park, J. H. Jo, L.-Y. Kuo, P. Kaghazchi and S.-T. Myung, *ACS Appl. Mater. Interfaces*, 2018, 10, 40978-40984.
- [26] H.-H. Ryu, N.-Y. Park, J. H. Seo, Y.-S. Yu, M. Sharma, R. Mücke, P. Kaghazchi, C.-S. Yoon and Y.-K.

Sun, *Materials Today*, In press, <https://doi.org/10.1016/j.mattod.2020.01.019>

[27] K. Meier, T. Laino and A. Curioni, *J. Phys. Chem. C*, 2014, 118, 6668-6679.

[28] D. O. Shin, K. Oh, K. M. Kim, K.-Y. Park, B. Lee, Y.-G. Lee and K. Kang, *Scientific reports*, 2015, 5, 1805.

[29] B. Andriyevsky, K. Doll and T. Jacob, *Mater. Chem. Phys.*, 2017, 185, 210-217.

[30] S. Yu, R. D. Schmidt, R. Garcia-Mendez, E. Herbert, N. J. Dudney, J. B. Wolfenstine, J. Sakamoto and D. J. Siegel, *Chem. Mater.*, 2016, 28, 197-206.

[31] X. Zhan, S. Lai, M. P. Gobet, S. G. Greenbaum and M. Shirpour, *Phys. Chem. Chem. Phys.*, 2018, 20, 1447-1459.

[32] M. Kubicek, A. Wachter-Welzl, D. Rettenwander, R. Wagner, S. Berendts, R. Uecker, G. Amthauer, H. Hutter and J. Fleig, *Chem. Mater.*, 2017, 29, 7189-7196.

[33] S. KC, R. C. Longo, K. Xiong and K. Cho, *Solid State Ionics*, 2014, 261, 100-105.

[34] A. Moradabadi and P. Kaghazchi, *Solid State Ionics*, 2019, 338, 74-79.

[35] P. Canepa, J. A. Dawson, G. S. Gautam, J. M. Statham, S. C. Parker and M. S. Islam, *Chem. Mater.*, 2018, 30, 3019-3027.

[36] S. Yu and D. J. Siegel, *Chem. Mater.*, 2017, 29, 9639-9647.

[37] S. Panahian Jand and P. Kaghazchi, *MRS Communications*, 2018, 8, 591-596.

[38] J. P. Perdew, K. Burke, and M. Ernzerhof, *Phys. Rev. Lett.* 1996, 77, 3865-3868

[39] J. W. Sun, A. Ruzsinszky, and J. P. Perdew, *Phys. Rev. Lett.* 2015, 115, 036402.